Macromolecular Research, Vol. 20, No. 6, pp 605-613 (2012)
DOI 10.1007/s13233-012-0087-1

www.springer.com/13233
pISSN 1598-5032 eISSN 2092-7673

An Effective Method for Manufacturing Hollow Carbon Nanofibers and Microstructural Analysis

Byoung-Sun Lee[1], Kyu-Min Park[1], Woong-Ryeol Yu*[,1], and Ji Ho Youk[2]

[1]*Department of Materials Science and Engineering, Seoul National University, Seoul 151-742, Korea*
[2]*Department of Advanced Fiber Engineering, Division of Nano-Systems, Inha University, Incheon 402-751, Korea*

Received June 24, 2011; Revised October 4, 2011; Accepted October 27, 2011

Abstract: Hollow carbon nanofibers (HCNFs) were successfully manufactured by *co*-axial (core/shell) electrospinning of poly(styrene-*co*-acrylonitrile) (SAN) and poly(acrylonitrile) (PAN) solutions. The shell component (PAN) was converted into a turbostratic carbon structure by thermal treatment, whereas the *sacrificial* core component (SAN) was eliminated. SAN was found to be a very suitable material for the *sacrificial* core. SAN exhibited excellent *co*-axial electrospinnability to produce a uniform core/shell nanofiber precursor because of its immiscibility with PAN. Also, SAN had a good thermal sustainability that prevented the PAN shell from shrinking during the stabilization and carbonization processes, thus maintaining the shell structure. These two predominant properties of SAN enabled the manufacturing of uniform HCNFs with controlled inner diameters and wall thickness that ranged from 120-510 nm and 52-145 nm, respectively. The core solution properties, such as solution concentration and flow rate, were mostly effective in controlling both the outer diameters and the wall thicknesses of HCNFs. The microstructure of these HCNFs was investigated using high resolution transmission electron microscopy. The crystallite size and crystallinity of HCNFs were dependent on their wall thicknesses. As the wall thicknesses of HCNFs decreased, they developed smaller crystallites and higher crystallinities.

Keywords: hollow carbon nanofibers, *co*-axial electrospinning, core/shell nanofibers, turbostratic carbon.

Introduction

As new multifunctional materials, carbon nanomaterials, such as carbon nanotubes (CNTs) and graphene, exhibit excellent mechanical and electrical properties.[1,2] Carbon nanofibers (CNFs) with short-range ordered graphitic structures are one of such carbon nanomaterials. They have usually been manufactured by using one of two routes: chemical vapor deposition[3-5] or electrospinning and subsequent carbonization.[6-10] The former produces CNFs with hollowed and relatively perfect microstructures.[4] The resulting CNFs are only a few microns in length and have small diameters. On the other hand, the latter method can produce continuous CNFs with relatively imperfect microstructures but with a wide range of diameters and long lengths.[6] Since the electrospinning and subsequent carbonization method allows the fabrication of a variety of CNFs, such as hollowed or multilayered CNFs,[9] it has been widely employed to develop multi-functional CNFs for battery electrodes[11] and super capacitors.[12]

Early studies on CNFs were dedicated to developing solid CNFs by electrospinning PAN and subsequent carbonization.[13,14] The mechanical properties of solid CNFs were characterized using either a single CNF[6] or their assembled mat forms.[15] The modulus and strength of a single CNF are ~60 and 0.90 GPa, respectively, while ~6 GPa and ~160 MPa are the respective values for mat form CNFs. Chasiotis *et al*. recently prepared strong CNFs with modulus and tensile strength of 170±40 and 3.5±0.6 GPa, respectively.[16] To utilize their axial mechanical properties, various attempts have been made to produce aligned CNFs with limited success.[7,17] Recently, nano-tailoring of CNFs using either CNTs or metal/ceramic nanoparticle incorporation was investigated due to their excellent electrical properties,[7,11,18,19] thus enlarging their applications to Li-ion batteries and super capacitors.[11,12,19]

Emulsion electrospinning was emerged as an effective method to fabricate porous carbon nanofibers,[20] though the control of the pore size and distribution was not proven. The monotonic and uniform holes on each carbon nanofiber including their size control are often required to develop multi-functional hollow carbon nanofibers incorporating nanoparticles. In this aspect, *co*-axial electrospinning of core/shell nanofibers and subsequent carbonization method (during which core components are eliminated) can be regarded as an effective manufacturing method for hol-

*Corresponding Author. E-mail: woongryu@snu.ac.kr

lowed CNFs (HCNFs).[9] HCNFs were originally designed to develop multi-functional materials by incorporating nanoparticles into the core for a specific function. Some examples include fluidic delivery[21] and metal core-carbon shell composite for Li-ion battery applications.[22] However, these methods met serious problems to obtain HCNFs with high morphological quality (uniformity of hollowness and shell thickness, as well as reproducibility) mainly due to both the material composition and the uncontrolled *co*-axial electrospinning process.[23]

In this study, we report a new material composition and the corresponding process for HCNFs with high morphological quality (we defined 'high quality' as uniform hollowness and uniform wall thickness for HCNFs). For these HCNFs, uniform precursors, *i.e*., core/shell nanofibers, have to first be prepared. We found that besides the electrospinning conditions, such as solution concentrations, applied voltage, and tip-to-collector distance, the choice of a suitable sacrificial core material is the most important factor for preparing uniform core/shell electrospun nanofibers. The sacrificial core has to be sustainable up to certain temperatures during the carbonization of the shell component; otherwise the shell would shrink irregularly. In this study, poly(styrene-*co*-acrylonitrile) (SAN) was found to satisfy this requirement. Various HCNFs were manufactured using the new composition (SAN and PAN) and the concentration effect of the SAN and PAN solutions on the HCNF morphologies and microstructures were systematically investigated.

Experimental

Materials. SAN (M_w=120,000 g/mol, acrylonitrile 28.5 mol%) and PAN (M_w=200,000 g/mol) were purchased from Cheil industries and Misui chemical, respectively. Poly (methyl methacrylate) (PMMA) (M_w=996,000 g/mol) and heavy mineral oil were purchased from Sigma Aldrich. *N*,*N*-dimethylformamide (DMF, 99.5%) and acetone were used as solvents. SAN and PAN were dissolved in DMF. Their concentrations were varied as shown in Table I.

Fabrications of CNFs and HCNFs. CNFs were fabricated to investigate the carbonization behavior of PAN nanofibers. PAN was dissolved in DMF at a concentration of 16 wt%, ultrasonicated for 5 h, and then stirred at 80 °C for 5 h. The electrospinning conditions were set up as follows: applied voltage of 20 kV, tip-to-collector distance (TCD) of 10 cm, and solution flow rate of 0.5 mL/h. The PAN nanofibers were then carbonized by a continuous thermal treatment that included stabilization and carbonization processes. The stabilization was conducted at 270-300 °C for 1 h under an air atmosphere, while subsequent carbonization was carried out at 1000 °C for 1 h under a nitrogen atmosphere. The temperature was increased at a rate of 10 °C/min (Figure 1).

A *co*-axial nozzle with two concentric cylinders was designed to make core/shell nanofibers (Figure 2). The *co*-axial electrospinning conditions were set up based on preliminary experiments (Table I). Three groups of samples were prepared. Group 'F' was designed to investigate the effect of the flow rate, in particular, of the core solution on the morphologies of HCNFs, while groups 'C' and 'S' were prepared to investigate the concentration effect of the core and shell solutions, respectively. All these core/shell nanofibers were converted into HCNFs using the same thermal treatment conditions as shown in Figure 1.

Characterizations. FTIR (FT/IR 6300, Jasco) analysis

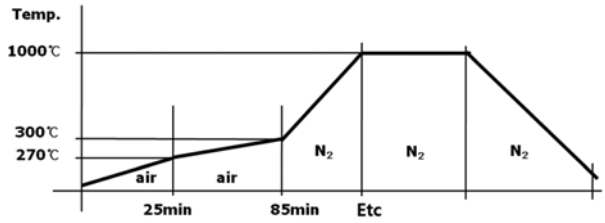

Figure 1. Continuous thermal treatment of PAN nanofibers for their stabilization and carbonization.

Table I. *Co*-Axial Electrospinning Conditions for Various HCNFs

Group	Sample Code	Solutions (wt%)		Flow Rate (mL/h)		Applied Voltage (kV)	TCD (cm)
		Core (SAN)	Shell (PAN)	Core	Shell		
F (Flow Rate)	F-1	30	20	0.1	1	18	15
	F-2			0.3			
	F-3[a]			0.5			
C (Core)	C-1	20	20	0.5	1		
	C-2	25	20				
	C-3[a]	30	20				
S (Shell)	S-1	30	10	0.5	1		
	S-2	30	15				
	S-3[a]	30	20				

[a]Note that F-3, C-3, and S-3 are the same condition.

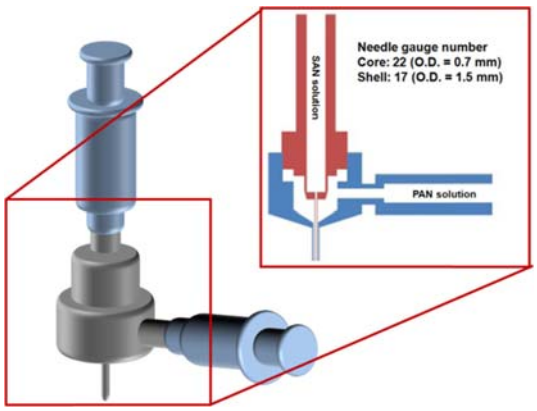

Figure 2. Schematic drawings of a syringe needle system for *co*-axial electrospinning (O.D. represents the outer diameter).

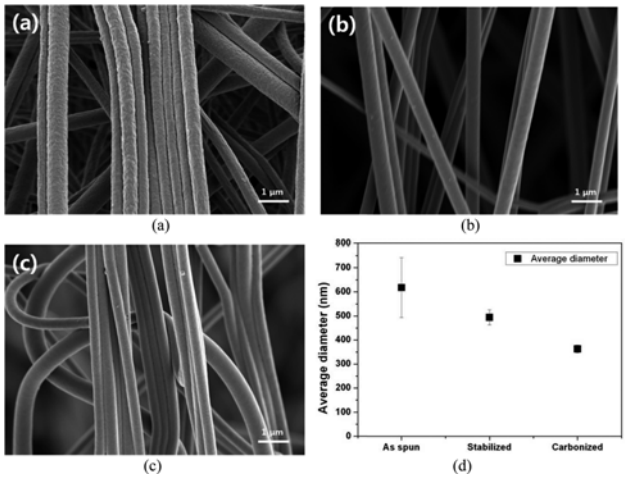

Figure 3. SEM images of (a) as-spun, (b) stabilized and (c) carbonized PAN nanofibers, and (d) their average diameters.

was conducted to investigate the micro-structural change of the core/shell nanofibers during the stabilization and carbonization processes. Raman spectroscopy (Ar laser, wave length: 514 nm, T64000, HORIBA) and wide angle X-ray diffraction (WAXD) (GADDS, Bruker) were also employed to characterize the carbonized structures of HCNFs. The tubular structures and morphologies of HCNFs were investigated using both a field emission scanning electron microscope (FE-SEM) (SUPRA 55VP, Carl Zeiss and JSM-6700F, Jeol) and a transmission electron microscope (TEM) (JEM 1010, Jeol). The microstructures of HCNFs were investigated using a high resolution transmission electron microscope (HR-TEM, JEM-3000F).

Results and Discussion

Prerequisites of the Core Material. It is important to choose suitable sacrificial core materials for HCNFs. To understand the prerequisites for the sustainability of core materials during the carbonization process, the carbonization behavior of PAN nanofibers prepared by single nozzle electrospinning were first investigated. Figure 3 shows the morphologies of as-spun, stabilized, and carbonized PAN nanofibers. In order to observe their diameter change during thermal treatment, PAN nanofibers with large diameters were prepared. The average diameters of electrospun nanofibers strongly depend on the PAN concentration.[15] After thermal treatment, the diameters of the PAN nanofibers decreased. The average diameters of the stabilized and carbonized nanofibers were about 80% and 60% of that of as-spun nanofibers, respectively. This shrinkage behavior was caused by micro-structural changes, such as ring formation and combination into the graphitic layers. If a sacrificial core is decomposed at an early stage of the thermal treatment, the shell components of HCNFs will experience severe shrinkage without any support such that their shapes may be distorted. Therefore, it can be postulated that thermally sustainable material is a better sacrificial core because it can support the shell layer during the thermal treatment.

Three materials (PMMA, heavy mineral oil, SAN) were compared for core materials. PMMA begins thermal decomposition below 300 °C.[24] Although the thermal decomposition occurs in the temperature range of 200-400 °C, it dominantly proceeds below 300 °C. As the carbonization of the PAN shell progresses, the PMMA core will be thermally decomposed before the stabilization of PAN, resulting in a collapsed hollow structure due to the thermal shrinkage of the PAN shell. The mineral oil exhibits similar behavior to PMMA due to the onset of thermal decomposition below 300 °C. Furthermore, it is not easy to control its viscosity for successful electrospinning. Thermal decomposition behavior of SAN was investigated. Figure 4 shows that its thermal decomposition takes place at over 350 °C, implying that SAN could maintain its original shape without thermal decomposition during the stabilization and early carbonization process.

The miscibility of the SAN solution with the PAN solu-

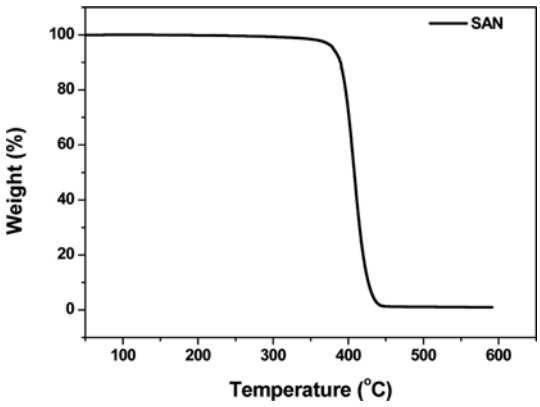

Figure 4. TGA curve of SAN measured at a rate of 10 °C/min.

Figure 5. Mixing behavior of the PMMA and SAN solutions with the PAN solution. (a) as- poured and (b) after one day.

tion was investigated. A simple method was adopted: pouring the PMMA (10 wt%) and SAN (30 wt%) solutions into respective PAN solution, respectively (Figure 5). Upon being poured, the PMMA solution formed a mixed interface with the PAN solution and the solutions became homogeneous with time, whereas the SAN solution maintained a clearly separate interface for a considerably long period.

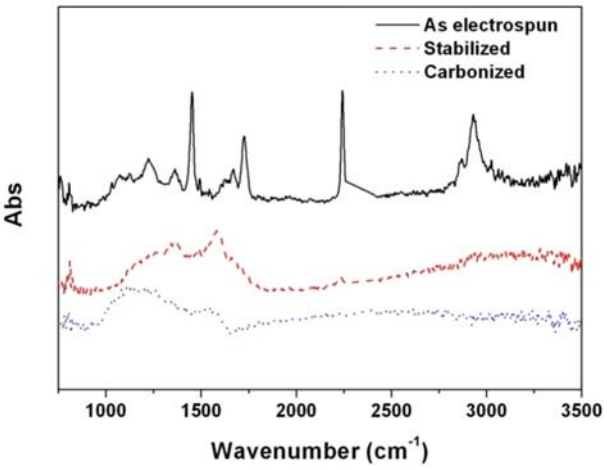

Figure 6. FTIR spectra of electrospun, stabilized, and carbonized core/shell nanofibers (C-3).

Since the mixed interface between the core and shell can result in irregular hollows and also disturb uniform electrospinning, SAN can be considered as a suitable sacrificial core material for manufacturing HCNFs.

Characterization of HCNFs. HCNFs (sample code C-3) were characterized using FTIR, WAXD, and Raman spectroscopy. Figure 6 shows the FTIR spectra of electrospun, stabilized, and carbonized hollow nanofibers (C-3). A characteristic peak at 2240 cm^{-1} associated with the -C≡N group disappeared after the stabilization process, indicating that the -C≡N group was transformed to -C=N (1700 cm^{-1}) by cyclization. In addition, the C-H peak at 2950 cm^{-1} disappeared by dehydrogenation, which is evidence of good stabilization. Note that both -C≡N and -C=N groups were not observed in the carbonized hollow nanofibers, while a peak around 1600 cm^{-1} clearly evolved, representing that the aromatic ring (carbon six-membered ring) was formed during the carbonization process. As a result, it can be concluded that the core/shell nanofibers were successfully converted to carbonized nanofibers.

Raman spectroscopy provides more strong evidence to confirm the carbonized structure in the HCNFs. The D peak in Figure 7(a) is related to the breaking of symmetry caused by structural disorders, such as in-plane substitution heteroatoms, vacancies, and grain boundaries, while the G peak represents the in-plane tangential stretch vibration mode (E_{2g}) of the graphite sheet.[25] The I_D/I_G ratio was 1.15, which is within reported values.[6,7] The microstructural imperfection could be improved by a graphitization process. The WAXD pattern shows the three equatorial peaks: primary (002), and secondary (10*l*) planes of the carbon graphitic layers (Figure 7(b)). The *d*-spacing value of the primary peak (2θ=24.4°) was calculated to be 0.364 nm, which is larger than that of graphite (0.335 nm), implying that the microstructure of HCNFs is a turbostratic carbon structure with a slightly mismatched layer-sequence.[26]

The microscopic images of the HCNFs (C-3) in Figure 8(a) and (b) clearly demonstrate that uniform and hollowed

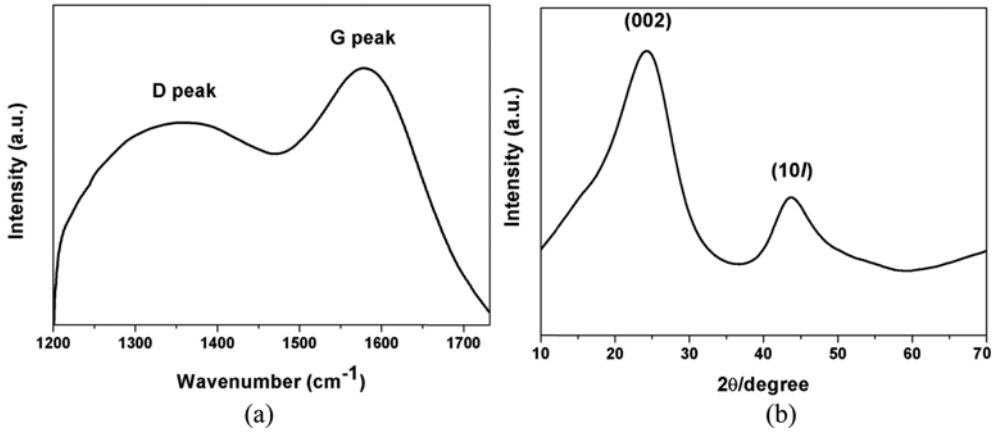

Figure 7. (a) Raman spectrum and (b) WAXD curve of HCNFs (C-3).

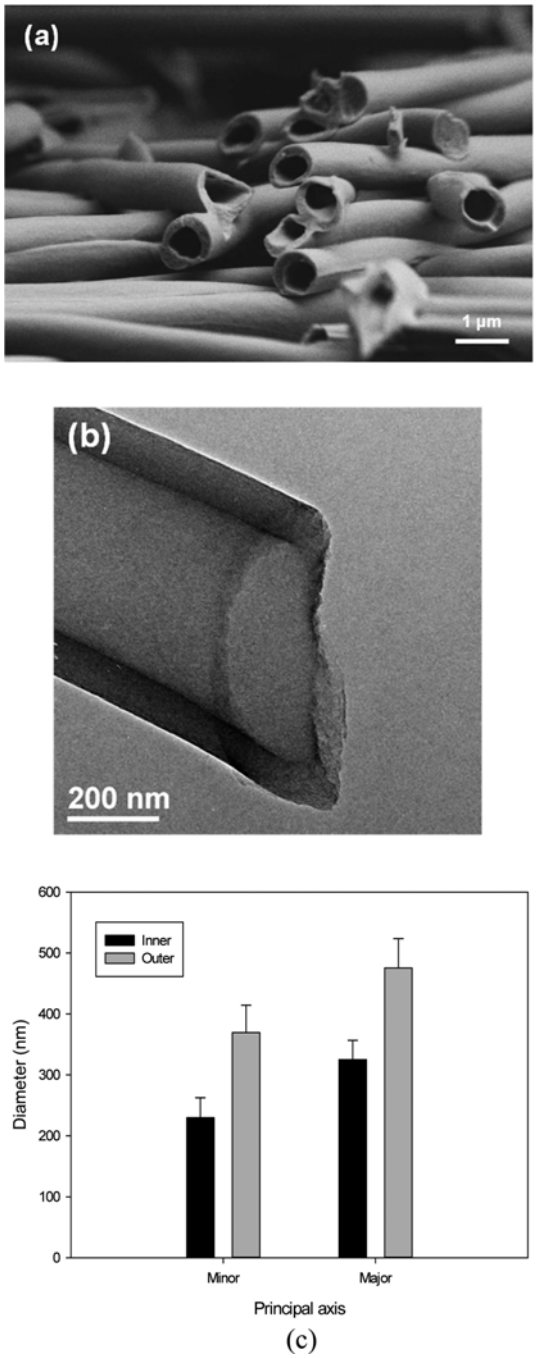

Figure 8. (a) FE-SEM and (b) TEM images of HCNFs (C-3) and (c) their elliptical cross-section.

CNFs were successfully manufactured and their cross-sections were elliptical. The inner and outer diameters on the major and minor axes were measured to characterize their elliptical cross-sectional shape, as shown in Figure 8(c). The values of eccentricity of the inner and outer boundaries were 0.50 and 0.64, respectively. Note that the eccentricity of an ellipse represents its similarity to a circle, *i.e.*, as the closer to zero the value of eccentricity is, the more circular in shape the ellipse becomes. The eccentricity of an ellipse is calculated by $\sqrt{1-b^2/a^2}$ where a and b are the lengths of major and minor axes on the ellipse, respectively. The elliptical cross-section shape of HCNFs is probably due to irregular interfacial tension between the core and shell solutions, the whipping and buckling phenomena during the electrospinning process, and/or the anisotropic shrinkage during the thermal treatment.[9] Nevertheless, the wall thicknesses on the major and minor axes are 144 and 134 nm (7% smaller), implying that the wall thickness of the HCNFs is reasonably uniform despite their elliptical shapes. To effectively describe the physical dimensions of HCNFs with the inner and outer elliptical boundaries, equivalent quantities can be defined. Provided that the equivalent diameter of an ellipse is defined as the diameter of a circle with the same area as that of the ellipse, the two equivalent (inner and outer) diameters can be used to represent the physical sizes of HCNFs. Corresponding equivalent wall thickness becomes half of the difference between two equivalent diameters. The equivalent wall thickness of the above HCNFs was 145 nm, which is reasonably close to the mean value (139 nm) of the two wall thicknesses (144 and 134 nm) along the major and minor axes. Hence, the equivalent quantities will be used to characterize the physical dimensions of HCNFs without stating 'equivalent' directly.

Investigation of HCNFs Manufacturing Conditions. To investigate the effect of the *co*-axial electrospinning conditions on HCNFs, three main manufacturing parameters (core flow rate, core concentration, and shell concentration) were varied. Firstly, the effect of the core flow rate on the hollow structure of HCNFs was investigated at a fixed flow rate (1 mL/h) and concentration (30 wt%) of the shell solution. The outer and inner diameters of the HCNFs increased as the core flow rate increased, whereas their eccentricities and wall thickness only slightly changed (Figure 9(a) and (d)). The increased flow rate supplies much more core material, resulting in the increased inner and thus outer diameters of HCNFs, but it resulted in similar wall thicknesses. The increased core concentrations resulted in similar behavior to that resulting from increased flow rates (Figure 9(b) and (e)).

Similar phenomena were observed according to the shell solution concentration, however, a couple of different trends were observed (Figure 9(c) and (f)). A dramatic change in both the wall thickness and eccentricity was observed as the shell concentration increased. The increased wall thickness can be explained by the increased polymer supply of the shell component, which may enlarge the outer diameter of HCNFs. On the other hand, both the inner and outer eccentricities of HCNFs were reduced, implying that a more circular shape was retained in HCNFs at increased shell concentrations. This may be due to a fact that the anisotropic thermal shrinkage of the shell component was relieved during the thermal treatment due to the thicker shell component. It is interesting to note that the inner diameter of the HCNFs also

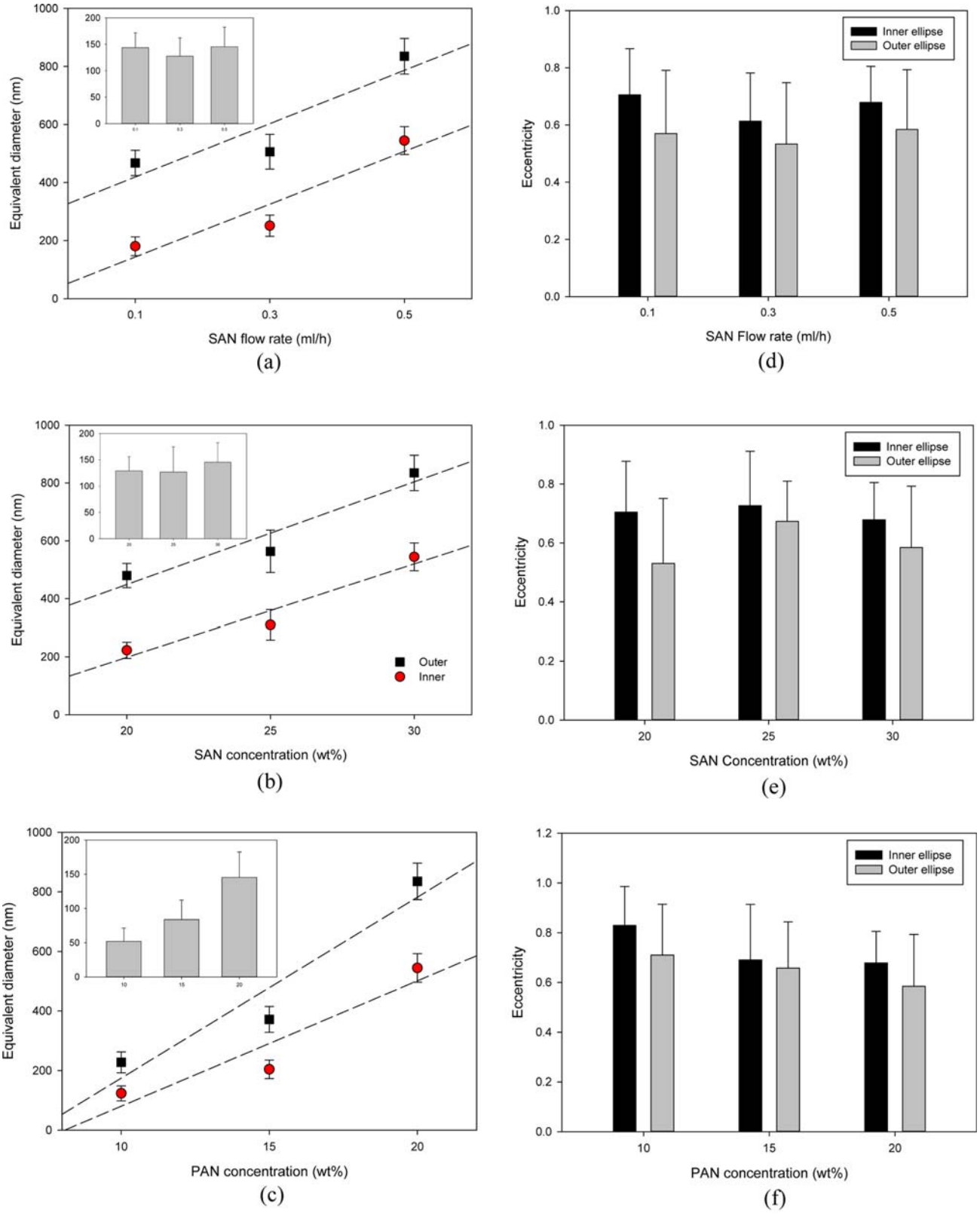

Figure 9. (a-c): the equivalent outer and inner diameters of HCNFs and (d-f) their eccentricities according to the manufacturing conditions. (a) and (d): SAN flow rate effect (0.1 to 0.5 mL/h), (b) and (e) SAN concentration effect (20 to 30 wt%), and (c) and (f) PAN concentration effect (10 to 20 wt%)). Note that the insect Figures in (a) through (c) represent equivalent wall thickness.

increased, even though the core solution properties were fixed. This can be explained by the solvent evaporation from the core solution, which may be disturbed by the increased supply of the shell, resulting in a less shrunk core during electrospinning. This core behavior may have caused the inner diameter of HNCFs to increase and the inner eccentricity to decrease as the shell concentration increased. It can be concluded from Figure 9 that the control of the core solution properties is an effective way to increase the physical dimensions (both the outer and inner diameters) of HCNFs without changing their wall thicknesses and eccentricities. The amount of the core supply and the evaporation speed of the core solvent are the crucial factors for determining the physical dimensions of the resulting HCNFs.

Microstructure of HCNFs. To investigate the microstructure of HCNFs, three samples (S-1, F-2, and S-3) were chosen. The first two samples were selected to directly compare their microstructures according to the shell concentrations. F-2 was used to examine the effect of the core solution property and its flow rate on the microstructure of the resulting HCNFs. Note that S-1, F-2, and S-3 are ordered with respect to physical dimensions (both the outer diameter and wall thickness). The morphological images and HR-TEM images of the selected HCNFs are shown in Figure 10. It is very clear from Figure 10(d) through (f) that a turbostratic carbon structure developed for all three samples, which is common

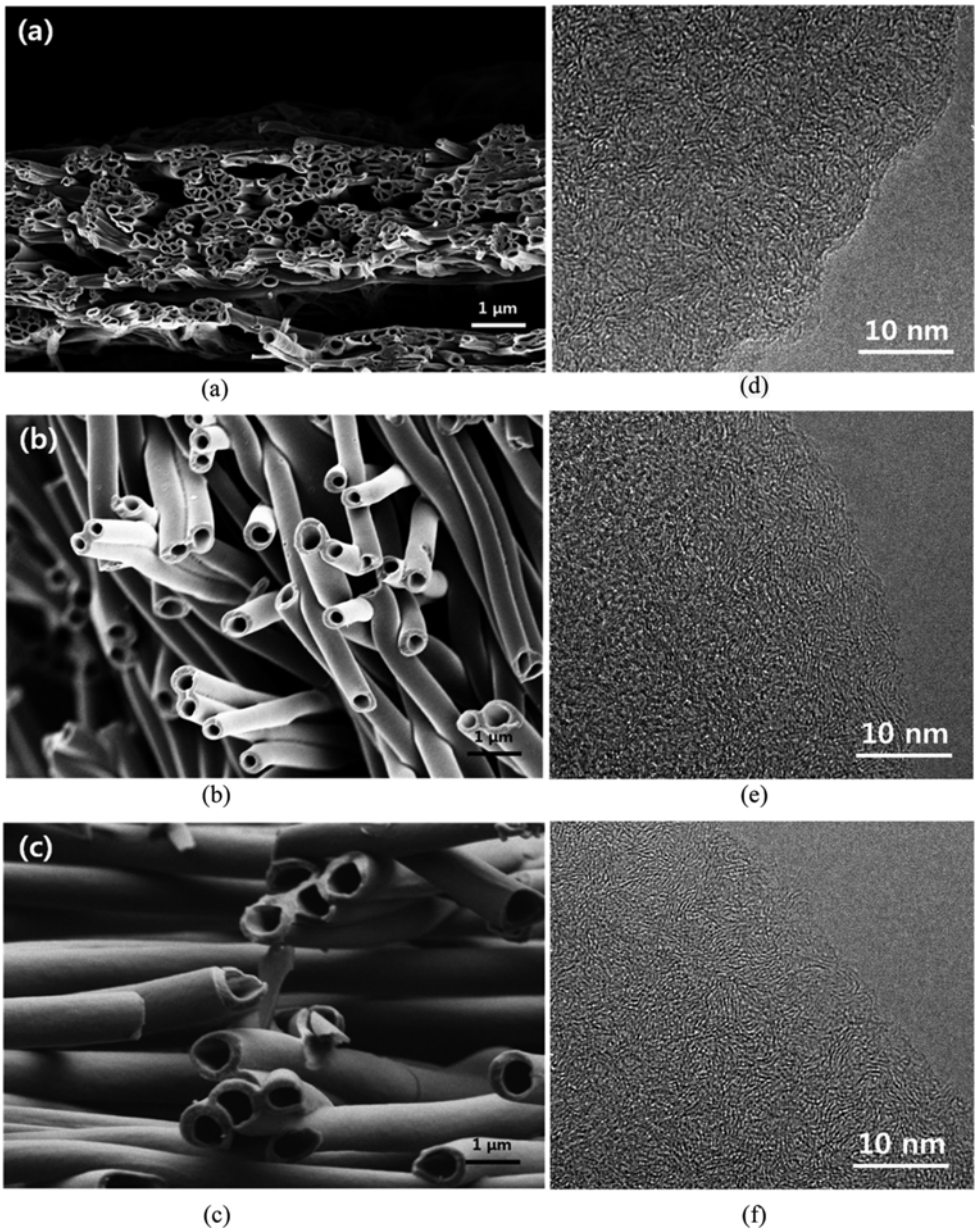

Figure 10. (a-c) SEM images of selected HCNFs and (d-f) their HR-TEM images. (a) and (d): S-1 (thinnest), (b) and (e): F-2 (moderate), (c) and (f): S-3 (thickest).

Table II. Microstructure of Selected HCNFs[a]

Sample Code	Outer Diameter (nm)	Wall Thickness (nm)	d_{002} (nm)	Crystallite Thickness (the number of layers, L_c)	Crystallite Size (L_a, nm)	Crystallinity (%)
S-1	227 (35)	52 (19)	0.356 (0.12)	3.4 (0.8)	1.13 (0.17)	42.7
F-2	505 (55)	127 (35)	0.346 (0.009)	4.2 (1.0)	2.38 (0.54)	37.9
S-3	835 (61)	145 (37)	0.342 (0.009)	4.6 (0.8)	4.56 (0.88)	36.2

[a]The parenthesis represents the standard deviation of the values.

for PAN based CNFs.[6,9,16] Note that higher carbonization temperatures than 1000 °C are used to induce clearer turbostratic carbon structure in PAN derived CNFs, however the carbonization temperature adopted in this study was also reported to induce such carbon structure.[6,16,27] Their crystal structures (crystallite thickness (L_c, the number of layers) and size (L_a) and crystallinity) were characterized using HR-TEM images and the results are summarized in Table II.

The L_c and L_a values of the HCNFs increased as the shell concentrations increased, while their crystallinities decreased (S-1 and S-3 in Table II). On the other hand, the F-2 sample, which was manufactured using the same solution concentration as S-3 but was electrospun using a different flow rate of the core solution, showed that its L_c, L_a, and crystallinity were positioned in-between those of S-1 and S-3. Since the wall thickness of F-2 is also in-between the S-1 and S-3 values, it can be postulated that the crystal structure of HCNFs are governed by their wall thicknesses. To further investigate this deduction, a crystal density (the number of crystallites per unit length) of the HCNFs was calculated using their wall thickness values, crystallite sizes, and crystallinities. Firstly the volume of a crystallite was calculated by assuming that its shape was a thin coin with a diameter and height of the crystallite size and thickness, respectively. The crystallite density was then calculated by multiplying the crystallinity by the cross-section area of the HCNFs and dividing it by the volume of a crystallite. The crystallite densities of the three HCNFs (S-1, F-2, and S-3) were 8.30×10^3, 7.08×10^3, and 3.53×10^3 per unit length (nm) of the HCNFs, respectively. Since the crystallite density is an equivalent quantity to the nuclei density, it can be concluded that the number of nuclei, which were formed during the thermal treatment, increased as the wall thicknesses of the HCNFs decreased. Furthermore, larger crystallites that were observed in thicker HCNFs can be explained by an afterward growth mechanism of the nuclei. Since the growth of the crystallites around the nuclei is supposed to interfere with neighboring nuclei, larger crystallites can be observed in HCNFs with lower nuclei density due to their fewer interventions. In conclusion, the experimental values in Table II support that the crystal structure of HCNFs are governed by their wall thickness.

Lastly, the crystal orientation in HCNFs was investigated using the reciprocal lattices in Figure 11(a) to (c). It is obvious that all of the three HCNFs have randomly oriented crystallites. This may be due to the unconstrained thermal treatment. During the thermal treatments, thermal shrinkage occurred and the crystallites might have rotated and formed into a randomly oriented configuration. If tension is applied during the thermal treatment, the crystallites may be oriented as observed in commercial carbon fibers.[28] Diffused rings can be observed in S-1 (with high crystallinity and nuclei density), while the other two samples show clear and sharp rings. As explained in the above paragraph, the crystal growth of a nucleus in S-1 is disrupted by its many neighboring nuclei, causing many imperfect crystallites in that sample. On the contrary, the lower nuclei density in the other samples (F-2 and S-3) might bring about little intervention of the crystal growth of a nucleus in the HCNFs, resulting in relatively more perfect crystallites in these samples. These results support our claim once more that the crystal structures of HCNFs are governed by their wall thicknesses.

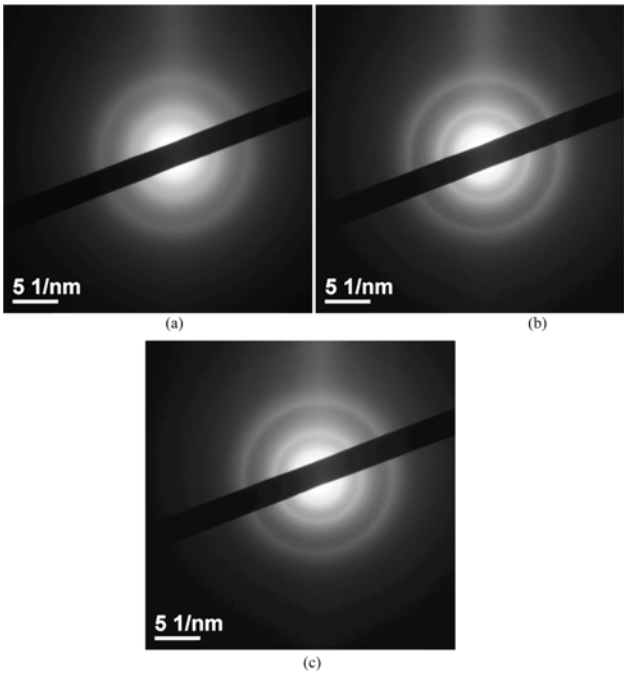

Figure 11. The reciprocal lattice patterns of (a) S-1, (b) F-2, and (c) S-3.

Conclusions

To manufacture uniform HCNFs using *co*-axial electrospinning and subsequent carbonization, two prerequisites (*co*-axial electrospinnability and thermal sustainability) are required. In this study, we found that SAN satisfied the two prerequisite conditions as a core material due to its immiscibility with PAN, good *co*-axial electrospinnability into core/shell nanofibers, and thermal sustainability during the carbonization process. A variety of HCNFs were manufactured using the new composition (SAN core/ PAN shell), demonstrating that the current system is highly suitable for uniform and controlled HCNFs. Parametric experiments showed that the core solution properties (concentration and flow rate) are the main factors in controlling both the diameters and the wall thicknesses of HCNFs. The crystal (turbostratic carbon) structure of HCNFs was found to be dependent on wall thickness. HR-TEM analysis supports this result by showing that HCNFs with thinner wall thicknesses had smaller crystallites but higher crystallinity.

Acknowledgement. This research was supported by Basic Science Research Program through the National Research Foundation of Korea (NRF) funded by the Ministry of Education, Science and Technology (2010-0022633).

References

(1) J. P. Salvetat, J. M. Bonard, N. H. Thomson, A. J. Kulik, L. Forró, W. Benoit, and L. Zuppiroli, *Appl. Phys. A: Mater.*, **69**, 255 (1999).
(2) S. Gilje, S. Han, M. Wang, K. L. Wang, and R. B. Kaner, *Nano Lett.*, **7**, 3394 (2007).
(3) V. I. Merkulov, A. V. Melechko, M. A. Guillorn, D. H. Lowndes, and M. L. Simpson, *Appl. Phys. Lett.*, **79**, 2970 (2001).
(4) G. Che, B. B. Lakshmi, C. R. Martin, E. R. Fisher, and R. S. Ruoff, *Chem. Mater.*, **10**, 260 (1998).
(5) K. B. K. Teo, S.-B. Lee, M. Chhowalla, V. Semet, V. T. Binh, O. Groening, M. Castignolles, A. Loiseau, G. Pirio, P. Legagneux, D. Pribat, D. G. Hasko, H. Ahmed, G. A. J. Amaratunga, and W. I. Milne, *Nanotechnology*, **14**, 204 (2003).
(6) E. Zussman, X. Chen, W. Ding, L. Calabri, D. A. Dikin, J. P. Quintana, and R. S. Ruoff, *Carbon*, **43**, 2175 (2005).
(7) E. J. Ra, K. H. An, K. K. Kim, S. Y. Jeong, and Y. H. Lee, *Chem. Phys. Lett.*, **413**, 188 (2005).
(8) J. Liwen and Z. Xiangwu, *Nanotechnology*, **20**, 155705 (2009).
(9) E. Zussman, A. L. Yarin, A. V. Bazilevsky, R. Avrahami, and M. Feldman, *Adv. Mater.*, **18**, 348 (2006).
(10) C. Haifeng and S. Liangkui, *Acta Polym. Sin.*, **0**, 61 (2009).
(11) L. Ji and X. Zhang, *Carbon*, **47**, 3219 (2009).
(12) C. Kim and K. S. Yang, *Appl. Phys. Lett.*, **83**, 1216 (2003).
(13) S. Y. Gu, J. Ren, and G. J. Vancso, *Eur. Polym. J.*, **41**, 2559 (2005).
(14) M. Lallave, J. Bedia, R. Ruiz-Rosas, J. Rodríguez-Mirasol, T. Cordero, J. C. Otero, M. Marquez, A. Barrero, and I. G. Loscertales, *Adv. Mater.*, **19**, 4292 (2007).
(15) S. F. Fennessey and R. J. Farris, *Polymer*, **45**, 4217 (2004).
(16) S. N. Arshad, M. Naraghi, and I. Chasiotis, *Carbon*, **49**, 1710 (2011).
(17) D. Li, Y. Wang, and Y. Xia, *Nano Lett.*, **3**, 1167 (2003).
(18) C. Kim, S.-H. Park, J.-I. Cho, D.-Y. Lee, T.-J. Park, W.-J. Lee, and K.-S. Yang, *J. Raman Spectrosc.*, **35**, 928 (2004).
(19) L. Ji and X. Zhang, *Electrochem Commun*, **11**, 795 (2009).
(20) C. Kim, Y. I. Jeong, B. T. N. Ngoc, K. S. Yang, M. Kojima, Y. A. Kim, M. Endo, and J. W. Lee, *Small*, **3**, 91 (2007).
(21) R. Srikar A. L. Yarin, and C. M. Megaridis, *Nanotechnology*, **20**, 275706 (2009).
(22) Y. Yu, L. Gu, C. Wang, A. Dhanabalan, P. A. van Aken, and J. Maier, *Angew. Chem. Int. Ed.*, **48**, 6485 (2009).
(23) A. K. Moghe and B. S. Gupta, *Polym. Rev.*, **48**, 353 (2008).
(24) J. D. Peterson, S. Vyazovkin, and C. A. Wight, *J. Phys. Chem. B*, **103**, 8087 (1999).
(25) B.-S. Lee and W.-R. Yu, *Macromol. Res.*, **18**, 162 (2010).
(26) A. Ōya and H. Marsh, *J. Mater. Sci.*, **17**, 309 (1982).
(27) M. S. A. Rahaman, A. F. Ismail, and A. Mustafa, *Polym. Degrad. Stab.*, **92**, 1421 (2007).
(28) M. K. Jain and A. S. Abhiraman, *J. Mater. Sci.*, **22**, 278 (1987).